

Fracture and Contact Adhesion Energies of Mica-Mica, Silica-Silica, and Mica-Silica Interfaces in Dry and Moist Atmospheres

Kai-Tak Wan

Department of Physics and Astronomy, University of Maryland, College Park, Maryland 20742

Douglas T. Smith[†] and Brian R. Lawn^{*‡}

Ceramics Division and Materials Science and Engineering Laboratory,
National Institute of Standards and Technology, Gaithersburg, Maryland 20899

A study is made of the factors that contribute to the energy of mica-mica, silica-silica, and mica-silica interfaces in the presence of moist atmospheres. Energies are measured using brittle fracture and contact adhesion techniques. Both "virgin" and "healed" interfaces are investigated, with special attention on the latter. The fracture and adhesion data overlap, reflecting a common underlying separation process by "sharp-crack propagation." The study identifies several contributors to the interface adhesion energies. At virgin mica-mica and silica-silica interfaces the energy is determined by primary ionic-covalent attraction, and by the screening of this attraction by condensed moisture from the atmosphere. At healed interfaces the energy depends on both environmental interaction and "lattice" coherence. At retracted cracks in mica-mica most of the virgin ionic attraction is retained. On misorienting separated cleavage halves prior to recontact the interaction energy drops substantially: in "dry" atmospheres (relative humidity <5%) a portion of the Coulombic interaction persists in the form of "macroscopic domains" of electrostatic charge, attributable to long-range order in the cation sublattice; in "wet" atmospheres (relative humidity >50%) capillary forces dominate. The dissimilar mica-silica system exhibits the same dominance by capillary forces in wet atmospheres. However, in dry atmospheres the adhesion energy becomes inordinately high, from spontaneous transfer of electronic charge from one surface to the other. The implications of these observations concerning mechanical properties of brittle ceramics are discussed. [Key words: mica, silica, interfaces, fracture, adhesion.]

I. Introduction

THE adhesion at boundaries between like or unlike solids can be a critical factor in such areas as tribology, coating technology, strength of materials, and powder processing. The higher the interface energy, the stronger the mechanical "communication" between the two adjoining solid halves. For example, in reinforced composites a strong fiber/matrix interface facilitates transfer of shear stress, enabling the fiber to bear a portion of an applied load. Optimization of toughness, on the other hand, demands that the interface not be too strong, in order that debonding may occur, nor too small that the ensuing pullout occurs without dissipative frictional con-

straint. Accordingly, a knowledge of interface energy states, especially in the presence of environmental fluid species, is of interest in modern ceramics science.¹

The interface energy can be quantified by the Dupré work of adhesion W ,² i.e., the work per interface area to separate the solid halves in the presence of a specified environment from their initial state at intimate contact to infinity in a reversible process. For ceramics, the most direct methods of measuring this quantity, exemplified by a wealth of experimental data on mica, are those of brittle fracture³⁻¹⁶ and adhesive pull-off at Hertz-like contacts.¹⁷⁻²³ These two methods are in fact complementary, in that they both involve interfacial separation by some form of "crack" propagation. Of the two, fracture is less restrictive, enabling one to determine energies of chemically bonded "virgin," in addition to "healed," interfaces. At healed interfaces, interfacial occlusion of exotic molecules from the environment is generally unavoidable. With contact pull-off, the two surfaces must first be brought into contact, so that only healed interfaces can be studied. Moreover, unless very special care is taken with mutual alignment of the specimen halves,²⁴ the recontacted surfaces will lack atomic registry, corresponding to a state of "lattice" incoherency.

In this paper we use both fracture and adhesion techniques to measure the work of separation for recontacted like and unlike interfaces in mica and high-purity silica glass in "moist" and "dry" atmospheres, comparing (where possible) with values for virgin interfaces. Adhesion energies in the range $100 \text{ mJ} \cdot \text{m}^{-2}$ to $10 \text{ J} \cdot \text{m}^{-2}$ are recorded. In saturated atmospheres, capillary condensation of water at the open "crack" effectively screens any solid-solid interactions, so that the adhesion is dominated by the (negative) Laplace pressure.²⁵ At intermediate relative humidity the capillary retracts toward the crack front (contact circle), allowing the solid-solid forces to operate. These solid-solid forces have a strong ionic attraction in the like mica-mica system, with a "locked-in," correlated long-range component from disorder in the cationic lattice. This long-range component is not seen in the pure silica-silica system, although the presence of network-modifier cations (i.e., in soda-lime glass²⁶) can give rise to a similar ionic attraction. In the unlike mica-silica system the electrostatic interaction is dominated by transfer of free charge across the interface.²⁷ This latter electrostatic force is especially manifest in dry atmospheres. Broad conclusions concerning interface energies in solid junctions are drawn from the results, and implications concerning specific mechanical properties for brittle materials are discussed.

II. Experimental Section

(1) Materials Preparation

Muscovite mica and silica glass were chosen as model materials for this study because of the capacity to prepare speci-

T. A. Michalske—contributing editor

Manuscript No. 196618. Received June 25, 1991; approved November 7, 1991

Supported by the U.S. Office of Naval Research.

*Member, American Ceramic Society.

†Ceramics Division.

‡Materials Science and Engineering Laboratory.

mens as thin sheets with surfaces of near-atomic smoothness, thereby facilitating intimate contacts for interface adhesion measurements. All specimen surfaces in our study were formed at room temperature in a dust-free laboratory atmosphere at relative humidity 40% to 60%.

Mica for the fracture experiments was prepared by the cleavage of specimens $\approx 25 \text{ mm} \times 10 \text{ mm}$, thickness $\approx 50 \mu\text{m}$. "Good" cleavage produces surfaces with just a few atomic-scale steps. Recontacted interfaces were prepared after rotating fully separated cleavage halves through $\approx 10^\circ$. Some incomplete cleavages through virgin sheets were allowed to run back before complete separation, thereby forming a healed interface with high lattice coherence. Optical inspection of the surfaces after conducting the fracture experiments confirmed the absence of cleavage steps on the accepted specimens.

Mica for the adhesion experiments was prepared by cleaving sheets of typical thickness 2 to 6 μm which contained no atomic steps over areas on the order of $10 \times 20 \text{ mm}$. Specimens with typical dimensions $7 \times 10 \text{ mm}$ were then cut from the sheets and promptly adhered to a freshly cleaved mica backing sheet to protect them from contamination. While still on the backing sheet, an evaporated silver layer 50 nm thick was deposited on the exposed back surface of each specimen, as required by the interferometry technique discussed below.

Since fracture surfaces of silica cannot be produced to the requisite atomic smoothness, an alternative approach was adopted for the preparation of silica specimens for both the fracture and adhesion experiments.²⁸ Molten silica glass was blown into bubbles with wall thickness $< 10 \mu\text{m}$ and allowed to cool quickly under surface tension. Specimens were selected from near-flat fragments and were kept in adhesive contact either with a second silica sample or with a clean mica surface, again to prevent contamination. Profilometry traces on test specimens of these silica surfaces indicated an average roughness of $\approx 0.5 \text{ nm}$ over 30- μm traces. As with the mica, silica specimens for use in the adhesion experiments were silvered on their back surfaces.

Mica-glass junctions were similarly formed by recontacting silica glass fragments onto freshly cleaved mica.

Some auxiliary experiments were run to investigate potential effects of aging and surface chemistry. Freshly recontacted mica-mica and silica-mica interfaces were heat-treated at 120°C under vacuum for 20 h. Newly cleaved mica sheets were washed in aqueous HCl at pH 5 to replace surface potassium cations by hydronium ions, thus forming "hydrogen mica";²³ hydrogen-hydrogen (H-H) and hydrogen-potassium (H-K) mica interfaces were then formed.

(2) Fracture and Contact Adhesion Techniques

Double-cantilever-beam (DCB) fracture¹⁶ and crossed-cylinder contact adhesion²² experiments were performed on the above interfaces. The tests were conducted in environmental enclosures that allowed for atmospheric control over a relative humidity range $\text{RH} = 1\%$ to 100% . Time-dependent "crack" growth at constant applied loading was apparent in both the fracture and the contact adhesion configurations. Care was therefore taken to ensure that near-equilibrium conditions prevailed in all of the measurements below, by allowing the systems to settle down after each increment in applied load or displacement. Notwithstanding this care, crack growth in the driest environments, especially for the mica-mica and mica-silica systems, was notably erratic and irreproducible.

(A) *Fracture*: Fracture experiments were run on mica-mica and mica-silica systems by driving a thin steel wedge of thickness $2h = 50 \mu\text{m}$ along the interfaces.¹⁶ (Unfortunately, the glass fragments were too fragile for silica-silica experiments using this technique.) Crack lengths c were measured optically in transmitted light. The DCB crack system is highly stable, so equilibrium is rapidly approached after each incremental insertion of the wedge. Interface energies were calcu-

lated using the thin-beam formula for equilibrium cracks¹⁶

$$W = \frac{3h^2}{2c^4(1/E_1d_1^3 + 1/E_2d_2^3)} \quad (1)$$

with E_1 and E_2 Young's modulus and d_1 and d_2 the thickness of each specimen half, in the approximation of negligible mode II (shear) fracture. An effort was made to preserve "symmetry" by maintaining $E_1d_1^3 \approx E_2d_2^3$, so that the possibility of significant mode II contributions could be ignored.²⁹

(B) *Contact Adhesion*: Contact adhesion experiments were performed on recontacted mica-mica, silica-silica, and mica-silica couples, after gluing the specimens at their silver side, onto cylindrical silica lenses, radius of curvature R , for insertion into an Israelachvili-type surface force apparatus.²² The lenses were mounted with their axes at right angles in order that the undeformed surfaces were in contact at a point. The interferometer created by the silver layers (each approximately 95% reflecting) allows direct measurement of the surface separation profile, with 0.1- to 0.2-nm resolution in separation. When the surfaces are allowed to jump into contact under the action of their mutual attraction, they form a flattened contact circle of typical diameter 50 to 150 μm .

The adhesion energy, unless otherwise noted, was measured via the instability force, P_c , required to pull the surfaces apart from equilibrium separation; P_c is measured by the deflection of a double-cantilever spring supporting one of the cylindrical lenses. The spring constant of this force-measuring spring could be varied continuously over the range 10^2 to $10^5 \text{ N} \cdot \text{m}^{-1}$. Most adhesion data reported here were taken with the spring at $10^2 \text{ N} \cdot \text{m}^{-1}$ ("weak spring"); however, when the attractive force between the surfaces was relatively strong, as in the case of the silica-mica system at 1% RH, a setting of $10^5 \text{ N} \cdot \text{m}^{-1}$ ("stiff spring") was employed to minimize the effect of spring instability at small separations. For the pull-off adhesion measurements, the adhesion energy is related to P_c by

$$W = \frac{P_c}{\alpha\pi R} \quad (2)$$

where the coefficient α depends on the comparative radial dimensions of the contact circle and the adhesion zone (i.e., the interactive zone outside the contact circle where cohesion or adhesion forces operate): in the limit of small zones (dry atmospheres) $\alpha = 3/2$;¹⁷ for large zones (saturated atmospheres) $\alpha = 2$.¹⁸ The transition between these two limiting cases is discussed more fully elsewhere.¹⁹ We note that Eq. (2) is independent of elastic constants.

When the stiff spring is used, the pull-off measurement is no longer a practical method of determining W because, upon separation, the surfaces do not jump beyond the range of the adhesion force, making a measurement of P_c difficult. Under these circumstances, the force is measured as a function of surface separation, and these data are integrated to obtain W .

(3) Surface Charge Measurements

In the course of performing the contact adhesion experiments on the dissimilar mica-silica system in dry nitrogen, an unusually strong attractive force was observed after the surfaces had been in contact.³⁰ It was determined that the force was the result of electric charge transferred from one surface to the other, negative on the silica surface and positive on the mica.

A technique was developed³¹ to measure directly the amount of charge transferred in the contact adhesion experiment. Fine copper wires were attached to the evaporated silver layers on the back of each sample using pure indium as a solder. The silver layers were then held at ground potential through electrometer circuits; when the surfaces were separated, current flowed into or out of each silver layer (depending on the sign of the charge on the exposed surface) to create image charge layers. For separation large compared to the

substrate thicknesses, this image charge in each silver layer is equivalent to the charge left on the corresponding contact surface.

III. Results

Experimental results for interface energy W against relative humidity RH from the fracture and contact adhesion runs are plotted collectively as the data points in Figs. 1 to 5 for the mica-mica, silica-silica, and mica-silica systems, along with some comparative data from studies in the literature (as indicated in the captions). Data points for contact adhesion are computed using $\alpha = 2$ in Eq. (2). Points at the extreme right in these figures denote tests in bulk water. The fracture data are for three interface types: a first run through previously uncleaved virgin sheets (v); subsequent runs through interfaces healed in registry by retraction of an incompletely cleaved crack (h); subsequent runs through interfaces healed in misregistry by rotation of fully separated cleavage halves before recontact (h'). Contact adhesion data are for h' interfaces only. The data sets for each system include runs on several specimens. Curves through the data are theoretical fits from an analysis described in Section IV.

Observe that for those recontacted (h') interfaces in Figs. 1 to 5 where common fracture and contact adhesion results are available the data sets overlap each other within the broad scatter band. In this context, recall again that we have used $\alpha = 2$ in Eq. (2) to compute W for the contact adhesion energies, whereas in dry environments, where the capillary zone becomes negligibly small, $\alpha = 3/2$ is more appropriate.¹⁹ This latter modification will increase W for contact adhesion at low RH by some 33%, raising the appropriate data points in Figs. 1 to 5 (filled symbols) closer to the fracture data. This data overlap for h' interfaces implies complementarity between fracture and contact adhesion energetics, consistent with a common mechanism of separation by "crack" propagation.

Let us now consider each of the interface systems in turn.

(1) Mica-Mica Interface

The fracture and adhesion data shown in Fig. 1 for mica-mica show several characteristic features. For the fracture data, there are systematic downward shifts in W in going from v to h to h' interfaces. Generally, W diminishes

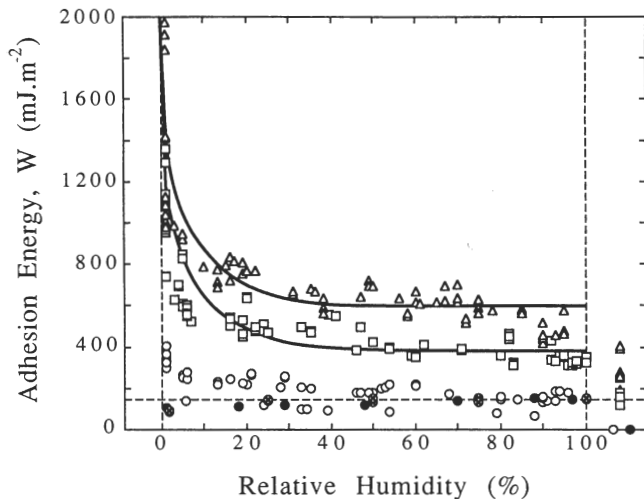


Fig. 1. Mica-mica interfaces, virgin (v —triangles), healed (h —squares), and recontacted (h' —circles), showing adhesion energy W as function of relative humidity RH. Results for: fracture experiments (open symbols), including data from an earlier study;²⁵ contact adhesion from current work (part-filled symbols) and from the literature²³ (filled circles). Data points at RH > 100% denote tests in bulk water. Horizontal dashed line at $W = W_{Lap} = 144 \text{ mJ} \cdot \text{m}^{-2}$ denotes work to separate against capillary forces. Curves are theoretical fits from Section IV.

monotonically with RH, albeit slowly for the h' interfaces. At low RH the decrease in W is somewhat abrupt, with considerable variability. At high RH the data set for each interface extrapolates to a level some 100 to 200 $\text{mJ} \cdot \text{m}^{-2}$ above the corresponding value in bulk water, implying the presence of a capillary.^{9,25} For h' interfaces the value of W in bulk water is close to zero, indicating an almost total negation of in-registry (v and h) solid-solid interactions by the liquid medium.

Figure 1 also shows values of W obtained in several adhesion experiments, including both current work and that of Christenson.²³ Within the scatter, these data agree with the h' fracture measurements for RH $\geq 50\%$, but fall below the capillary energy value for lower RH. As discussed above, this discrepancy is in part because the value $\alpha = 2$ is being used in Eq. (2) to compute W , while $\alpha = 3/2$ is more appropriate at low RH.¹⁹

While our main focus here is on h' interfaces, comparison with fracture data for h and v interfaces in Fig. 1 yields information on adhesion states associated with the intrinsic bonding.^{16,25} The upward translational shift from h' to h data sets over the full range of RH marks the onset of additional attractive long-range forces on bringing opposing solid surfaces into "lattice" registry. By contrast, observe the comparatively small shift from h to v data sets, suggesting that entrapment of water molecules (or other atmospheric species) at the healed interface is not strongly deleterious to the adhesion in mica.²⁵

Some additional results on mica-mica interfaces are shown in Figs. 2 and 3. Figure 2 shows fracture data for h and h' mica-mica healed interfaces subjected to aging at 120°C under vacuum prior to fracture, suggesting that aging is ineffective in modifying the interface structure in any significant way or even in dislodging occluded water. Within the scatter, there is little difference between these data and the h and h' data in Fig. 1. Figure 3 is for mica sheets acid-treated before recontact, to form hydrogen mica (H) from potassium mica (K) surfaces. Fracture data are for H-H and H-K recontacted interfaces. Also shown are adhesion data for the H-H mica interface from the literature.²³ Again, there is little difference between these h' data sets and those for the h' fracture of K-K mica in Fig. 1, suggesting that any residual attractive force is relatively insensitive to the actual cation species in the mica interlayer. Once more, it is the capillary that appears to control the adhesion.

(2) Silica-Silica Interface

Figure 4 for silica-silica shows data for h' surfaces from contact adhesion experiments, together with some data for

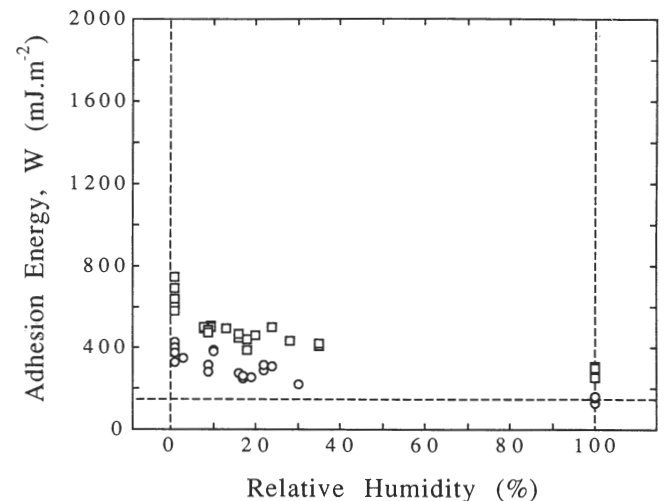


Fig. 2. Fracture data for mica-mica, W as function of RH, after aging healed (h —squares) and recontacted (h' —circles) interfaces at 120°C for 20 h. The horizontal dashed line is as in Fig. 1.

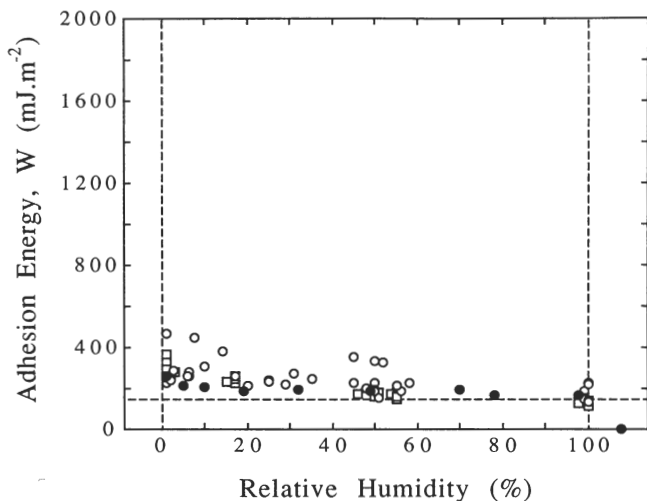


Fig. 3. Fracture data for mica-mica, W as a function of RH, surfaces acid-treated before recontact (h'). Fracture data shown are for hydrogen-hydrogen (H-H, open circles) and hydrogen-potassium (H-K, open squares) interfaces. Adhesion data for H-H interfaces, from the literature,²³ are also shown (filled circles). The horizontal dashed line is as in Fig. 1.

pure silica and soda-lime glass h interfaces from fracture experiments by Michalske and Fuller.²⁶ In these systems, W in bulk water is essentially zero (actually, slightly negative²⁸) for both h and h' interfaces. Now, however, W shows no significant increase with diminishing RH for the pure silica-silica system, suggesting a dominant capillary term over the entire data range. It is interesting to note that the comparative h -interface data for soda-lime glass from Michalske and Fuller²⁶ lie above their pure silica counterparts. Data for v interfaces are limited for fused silica, owing to the impractically slow crack velocities on approaching threshold in moist atmospheres. However, a value $W = 8 \text{ J} \cdot \text{m}^{-2}$ has been obtained in ultradry nitrogen gas, well in excess of the h and h' values of Fig. 4.³² Thresholds are not so inaccessible in soda-lime glass: estimates lie in the range $W = 1$ to $5 \text{ J} \cdot \text{m}^{-2}$.^{33,34}

By comparison with mica-mica in Fig. 1, the shift from h' to h data sets for silica-silica is negligibly small, from h to v (assuming $W^v = 1$ to $8 \text{ J} \cdot \text{m}^{-2}$) relatively large. This indicates

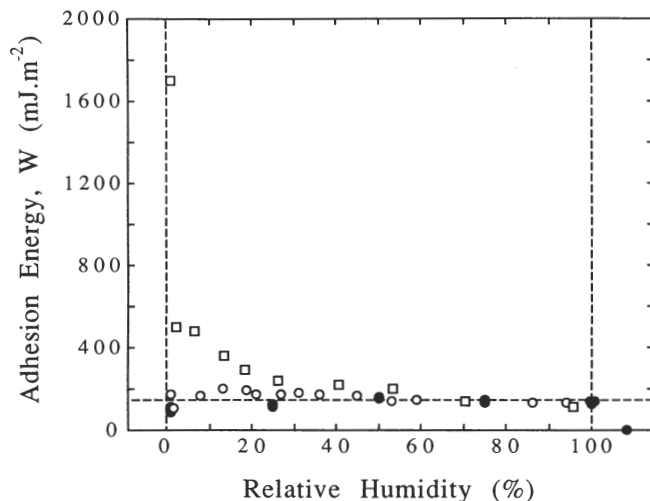


Fig. 4. Silica-silica interfaces, showing W as a function of RH. Data shown are contact adhesion data from present experiments (filled circles); and fracture data, healed (h —open circles) from the literature.²⁶ The point at RH > 100% denotes tests in bulk water. Also shown are data for healed soda-lime glass (open squares) from the literature.²⁶ Horizontal dashed line at $W = W_{Lap} = 105 \text{ mJ} \cdot \text{m}^{-2}$ denotes work to separate against capillary forces, taking into account the silica wetting angle of 45° .

saturation of primary siloxane bonds by water molecules³³ on first exposure to atmosphere, signifying a considerable negation of the primary adhesion from chemisorptive interaction with intrusive water molecules.³³ There is, however, a moderate $h \rightarrow h'$ shift for soda-lime glass, indicating some additional force associated with the presence of modifier cations in the glass network.²⁶

(3) Mica-Silica Interface

Figure 5 shows h' mica-silica data from both fracture and contact adhesion experiments. Analogous $h'-v$ (and thence $h'-h$) comparisons are not practicable at present; such comparisons would require preparation of chemically bonded "virgin" interfaces, e.g., by "sintering" the recontacted couples at temperatures well in excess of the 120°C limit of our experiments. Sintering studies to 450°C on healed cracks in soda-lime glass by Stavrinidis and Holloway³⁵ have demonstrated the feasibility of establishing (or re-establishing) strongly bonded interfaces in ceramic systems.

As was seen with the silica-silica interface, the data in Fig. 5 for the mica-silica system appear to be dominated by capillary forces over almost the entire RH data range, with significant deviation from the capillary value only at very low relative humidities (RH < 5%). However, considerably higher values of adhesion energy are observed for the lowest values of RH in both the fracture and adhesion experiments. This effect was first seen in the contact adhesion experiments³⁰ and has been shown to arise from the transfer of charge from one surface to the other when the surfaces are in contact.³¹ Because of the strength and long range (several micrometers) of the resulting electrostatic attraction between the surfaces, W was measured in the adhesion experiment at 1% RH using the "stiff spring" discussed in Section II(2). The force between the surfaces was measured as a function of separation from contact to separations $\approx 3 \mu\text{m}$, and these data were numerically integrated to obtain W ; three values between 4.7 and $6.4 \text{ J} \cdot \text{m}^{-2}$ were obtained for W . These results represent a lower limit for W , since the force between the surfaces at the largest separations studied, although small,

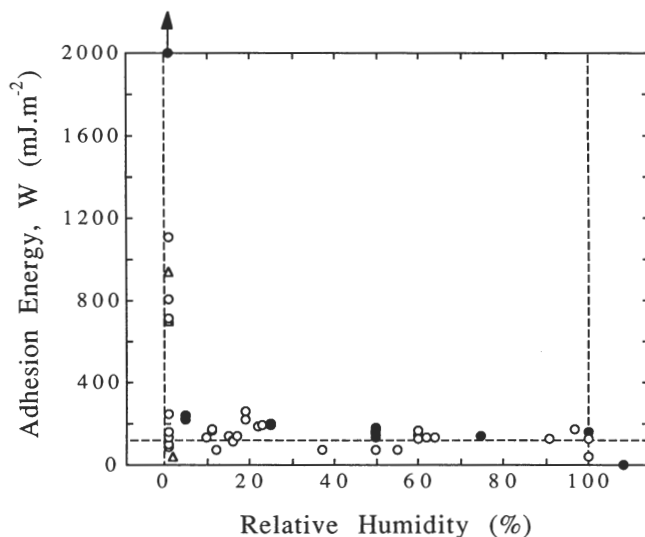


Fig. 5. Mica-silica interfaces, recontacted (h'), showing W as a function of RH. Data are for contact adhesion (filled circles), fracture (open circles), and fracture data on interfaces aged at 120°C for 20 h (open triangles). Data points at RH > 100% denote fracture and adhesion tests in bulk water. Horizontal dashed line at $W = W_{Lap} = 123 \text{ mJ} \cdot \text{m}^{-2}$ denotes work to separate against capillary forces, taking into account mica and silica wetting angles. In addition to the points shown, three measurements were made of the adhesion energy at 1% RH by integrating the force measured in the contact adhesion experiment between the surfaces from contact to large separation; these measurements yielded values of W of 4700 , 4700 , and $6400 \text{ mJ} \cdot \text{m}^{-2}$ (off-scale, but denoted by the arrow).

was still measurably nonzero. All other adhesion data in Fig. 5 were obtained by making pull-off measurements with the standard "weak-spring" technique, also discussed in Section II(2). More details of these measurements will be presented elsewhere.²⁷

The inclusion in Fig. 5 of W fracture data at low RH from aging cycles on mica-silica h' interfaces in dry environments again reveals no detectable differences from comparative data for unaged interfaces.

IV. Analysis and Discussion

We have presented results on interface energies for mica and silica in dry and moist atmospheres, like and unlike solid interfaces, using both adhesion and fracture experiments. In attempting to draw general conclusions from the data in the preceding section, we find it convenient to identify contributions to the adhesion^{36,37} from the primary bonding (B), macroscopic electrostatic domains (EI), and van der Waals (vdW) forces, as well as from capillary condensation (Lap), building on an earlier analysis.²⁵ We acknowledge that distinctions between these terms, especially primary (ionic) and electrostatic (charge domain) attractions in mica, are somewhat arbitrary, but they serve as a basis for analysis. Insofar as the different forces act independently, we may write the net adhesion energy as

$$W = W_B + W_{EI} + W_{vdw} + W_{Lap} \quad (3)$$

(I) Evaluation of Adhesion Energy Contributions

Of the terms in Eq. (3), that due to capillary condensation, W_{Lap} , is the most straightforward to evaluate.²⁵ Consider the crack interface in Fig. 6. The profile is defined by the separation $Y(X)$ at coordinate X along the interface, with $Y = b_0$ the lattice spacing (distance between cleavage-plane atom rows) at $X = 0$. Within the cylindrical meniscus of radius r a negative Laplace pressure acts to close the crack walls:

$$p_{Lap} = \frac{\gamma_{LV}}{r} \quad (4)$$

where γ_{LV} is the surface tension of water. The radius is given by the Kelvin equation

$$r = \frac{\gamma_{LV} \nu_M}{kT \ln(1/RH)} \quad (5)$$

with $\nu_M = 0.030 \text{ nm}^3$ the molecular volume of water, k Boltzmann's constant, and T the absolute temperature. For an equilibrium crack the appropriate adhesion energy is determined as the work to separate the two surfaces against the Laplace pressure²⁵

$$W_{Lap} = \int_{b_0}^{Y_K} p_{Lap}(Y) dY \quad (6)$$

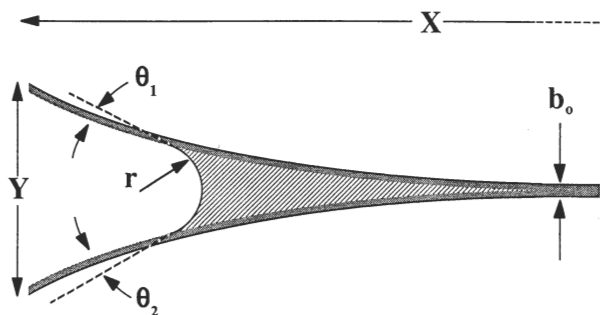


Fig. 6. Schematic representation of open crack or outer gap at crack interface between two lattice planes of initial separation b_0 . Capillary with Kelvin radius r and contact angles θ_1 and θ_2 are indicated. (X, Y) denote crack-plane coordinates.

with (ignoring crack-plane curvature)

$$Y_K = b_0 + r(\cos \theta_1 + \cos \theta_2) \quad (7)$$

the atom-plane separation at the meniscus. Substituting Eqs. (4) and (7) into Eq. (6) yields

$$W_{Lap} = \gamma_{LV}(\cos \theta_1 + \cos \theta_2) \quad (8)$$

This contribution is included as the dashed horizontal lines in Figs. 1 to 5, using $\gamma_{LV} = 72 \text{ mJ} \cdot \text{m}^{-2}$ for water, $\theta \approx 7^\circ$ (mica) and $\theta \approx 45^\circ$ (silica) from independent contact angle measurements. Of course, W_{Lap} is zero in a bulk liquid environment.

Thus, whereas W in Figs. 1 to 5 generally falls monotonically with moisture content, this trend is barely perceptible for the h' (recontacted) interfaces. In the limit of wet atmospheres ($RH \rightarrow 100\%$) the h' data, regardless of the specific solids on either side of the interface, or of any aging or chemical treatment of the constituent surfaces, tend closely to the dashed W_{Lap} lines. Recall that in bulk water, W for these same h' interfaces is close to zero. The implication is that any intrinsic solid-solid interactions are effectively screened out by the liquid condensate that fills the crack,²⁵ so that at $RH = 100\%$ capillary forces provide the dominant source of adhesion.

In the opposite limit of dry atmospheres ($RH < 5\%$), the h' adhesion energy in the untreated mica-mica system of Fig. 1 and the mica-silica system of Fig. 5 increases sharply. (Lack of data in this low RH region precludes a similar conclusion being drawn for the systems in Figs. 2 through 4.) High adhesion energies in these "inert" environments are associated with the intrinsic terms W_B , W_{EI} , and W_{vdw} . For intermediate humidities, the radius of the meniscus increases with increasing RH and the air-water interface moves from the crack tip toward the saturation configuration, as depicted in Fig. 7. Solid-solid attractions prevail over that portion of the crack interface outside the meniscus, and so diminish progressively as RH increases, as reflected most strongly in the virgin (v) and healed (h) mica-mica data of Fig. 1. Thus we need to evaluate the intrinsic adhesion in terms of a capillary screening model.

(A) *van der Waals Contribution:* The simplest of the three intrinsic adhesion terms is the contribution from van der Waals forces. This contribution is insensitive to lattice coherency, and is therefore the same for all interface types (v, h, h') in Figs. 1 to 5. The force-separation function for a

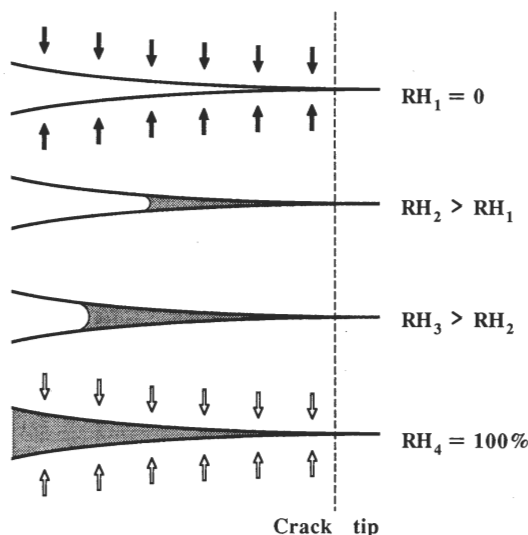


Fig. 7. Schematic showing how capillary fills crack at increasing RH. Within capillary, interaction governed by solid-liquid-solid forces (open arrows); outside capillary, by solid-solid forces (solid arrows). Liquid medium effectively screens forces, so interaction energy diminishes with increasing RH.

unit area of interface is of the form

$$p_{vdw}(Y) = \frac{H}{6\pi Y^3} \quad (9)$$

where H is a Hamaker constant.^{37,38} Now the Hamaker constant depends on whether X in Fig. 6 lies to the left (H_{SVS} , solid–vapor–solid) or right (H_{SLS} , solid–liquid–solid) of the meniscus. In conjunction with Eq. (7), the work to separate the two surfaces from an initial hard-wall spacing at $Y = b_0$ is²⁵

$$\begin{aligned} W_{vdw} &= \int_{b_0}^{\infty} p_{vdw}(Y) dY \\ &= \int_{b_0}^{Y_K} \frac{H_{SLS}}{6\pi Y^3} dY + \int_{Y_K}^{\infty} \frac{H_{SVS}}{6\pi Y^3} dY \\ &= W_{vdw}^1 \left\{ 1 - \frac{1}{[1 + r(\cos \theta_1 + \cos \theta_2)/b_0]^2} \right\} \\ &\quad + W_{vdw}^0 \left\{ \frac{1}{[1 + r(\cos \theta_1 + \cos \theta_2)/b_0]^2} \right\} \end{aligned} \quad (10)$$

with $W_{vdw}^0 = H_{SVS}/12\pi b_0^2$ and $W_{vdw}^1 = H_{SLS}/12\pi b_0^2$ the limits for interactions in air ($RH \rightarrow 0$, $r \rightarrow 0$) and liquid ($RH \rightarrow 1$, $r \rightarrow \infty$), respectively. From evaluations of these limiting solutions using the Hamaker constants in Table I,³⁸ in conjunction with the Kelvin relation in Eq. (5) and the values $b_0 = 0.34$ and 0.41 nm for mica and silica, respectively, Eq. (10) corresponds to a maximum value $W_{vdw} = 5 \text{ mJ} \cdot \text{m}^{-2}$ over the data range $RH = 1\%$ to 100% for the systems in Figs. 1 to 5, i.e., a comparatively small contribution.

(B) *Primary Bonding and Electrostatic Contributions:* The remaining terms in Eq. (3) which must dominate W for virgin interfaces require more detailed consideration. We consider these for the different solid–solid systems below.

Like Surfaces: We treat first interfaces between like solids, using *mica–mica* as our reference baseline. In muscovite mica the cleavage-plane bonding is principally ionic. It arises from Coulombic forces between positive interlayer potassium cations (or exchanged hydrogens) and negative sublayer charge from 1/4 occupancy of aluminum for silicon in adjacent silicate tetrahedra sheets.^{12,13,39–41} At this stage, let us assume that the potassiums are somehow “correlated” with the subsurface aluminum ions, and that the latter are stochastically distributed through the available sites. At the closed virgin interface, the potassium ions are recessed into hexagonal rings of oxygens. Upon separation, they attach to one or the other wall, depending upon the aluminum distribution. An array determined by a random number generator algorithm is depicted in Fig. 8. The resultant configuration is one of two surfaces with attractive $+/-$ charge cell clusters on opposite surfaces. The form of the force-separation function per unit area of mica interface from such Coulombic-cell interactions has been analyzed in the literature.^{7,8,42} Those analyses specifically consider a square checkerboard pattern with domains of linear dimension ℓ and charge density σ . The function may be written (Appendix)

$$p_B = \frac{32\sigma^2}{\pi^2 \epsilon \epsilon_0} \exp\left(-\frac{\sqrt{2} \pi Y}{\ell}\right) \quad (11)$$

with ϵ the dielectric constant of the intervening medium and ϵ_0 the permittivity of free space.

Now consider the intrusion of a capillary (Fig. 6). The appropriate dielectric constant in the force function of Eq. (11) depends on whether X lies to the left ($\epsilon = \epsilon_V$, vapor) or right ($\epsilon = \epsilon_L$, liquid) of the meniscus. Assuming that the only effect of the water is dielectric screening of the Coulombic forces, the work to separate the two *virgin* surfaces against

Table I. van der Waals Contribution to Interface Energy[†]

Solid–fluid–solid system	Hamaker constant ($\times 10^{-21}$ J)	Interaction energy ($\text{mJ} \cdot \text{m}^{-2}$)
Mica–air–mica	100	48
Mica–water–mica	22	10
Silica–air–silica	65	31
Silica–water–silica	8.3	4
Silica–air–mica	78	37
Silica–water–mica	10	5

[†]Using $b_0 = 0.34$ nm for mica and 0.41 for glass in Eq. (11).¹⁴ Hamaker constants from Ref. 38.

the forces in Eq. (11) is, for $\theta_1 = \theta_2 \approx 0$ in Eq. (7),

$$\begin{aligned} W_B &= \int_{b_0}^{\infty} p_B(Y) dY \\ &= \frac{32\sigma^2}{\pi^2 \epsilon_L \epsilon_0} \int_{b_0}^{Y_K} \exp\left(-\frac{\sqrt{2} \pi Y}{\ell}\right) dY \\ &\quad + \frac{32\sigma^2}{\pi^2 \epsilon_V \epsilon_0} \int_{Y_K}^{\infty} \exp\left(-\frac{2\sqrt{2} \pi Y}{\ell}\right) dY \\ &= \frac{16\sqrt{2} \sigma^2 \ell}{\pi^3 \epsilon_0} \exp\left(-\frac{\sqrt{2} \pi b_0}{\ell}\right) \\ &\quad \times \left[\frac{1}{\epsilon_L} + \left(\frac{1}{\epsilon_V} - \frac{1}{\epsilon_L}\right) \exp\left(-\frac{2\sqrt{2} \pi r}{\ell}\right) \right] \\ &= W_B^1 + (W_B^0 - W_B^1) \exp\left(-\frac{2\sqrt{2} \pi r}{\ell}\right) \end{aligned} \quad (12)$$

where $W_B^0 = (16\sqrt{2} \sigma^2 \ell / \pi^3 \epsilon_0 \epsilon_V) \exp(-\sqrt{2} \pi b_0 / \ell)$ and $W_B^1 = (16\sqrt{2} \sigma^2 \ell / \pi^3 \epsilon_0 \epsilon_L) \exp(-\sqrt{2} \pi b_0 / \ell)$ correspond to the limiting solutions for solid–solid interactions in inert atmosphere ($RH \rightarrow 0$, $r \rightarrow 0$) and liquid ($RH \rightarrow 1$, $r \rightarrow \infty$), respectively.

Evaluations of $W = W(RH)$ in Eq. (3) are made for the mica–mica virgin (v) interfaces in Fig. 1 using W_{Lap} , W_{vdw} , and W_B from Eqs. (8), (10), and (12), with $r = r(RH)$ from Eq. (5). At this stage we have implicitly assumed that the distribution of potassium ions on each surface is random, so that there are no electrostatic interactions from *macroscopic* charge domains, i.e., $W_{El} = 0$. The upper, solid curve is an appropriate fit to the v data, with the adjustments $\ell = 0.89$ nm, $W_B^0 =$

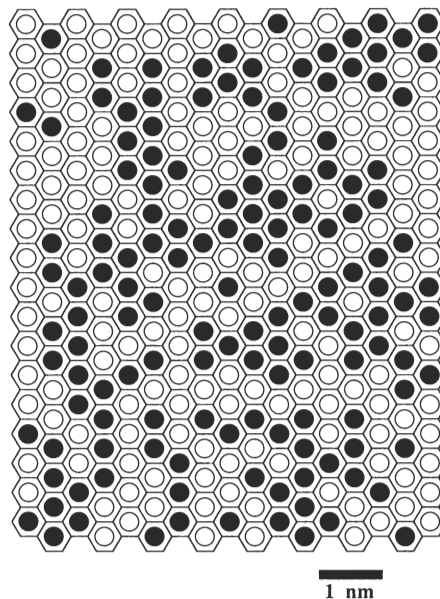


Fig. 8. Schematic of mica surface, showing distribution of potassium ions on a mica surface, as determined by a random number generator.

3020 mJ·m⁻², and $W_B^1 = 450 \text{ mJ} \cdot \text{m}^{-2}$ in Eq. (12). Assuming $\epsilon_V = 1.0$ for air, along with $b_0 = 0.34 \text{ nm}$ for mica, we use W_B^0 and ℓ to estimate a charge density $\sigma = 0.47 \text{ C} \cdot \text{m}^{-2}$, or ≈ 3 excess electronic charges per domain. The values of ℓ and σ appear to reflect the characteristic dimension and charge density of the potassium ion clusters in Fig. 8. However, the ratio $W_B^0/W_B^1 = \epsilon_L/\epsilon_V = 6.7$ implies $\epsilon_L = 6.7$ for the water within the capillary, which is low relative to the accepted value of 78 for bulk water. Noting the rapid falloff in the $W(Y)$ energy function in Eq. (12), corresponding to a factor of 2 reduction for opening displacements of less than one half the lattice parameter b_0 , this result could reflect a demonstrably strong solvation of water molecules at narrowly separated mica-mica surfaces.²¹

For *healed-coherent* (h) interfaces, W_B is simply diminished by an amount equal to the work to form an occluded layer, a "fault" energy, γ_h .^{16,25} The dashed line in Fig. 1, obtained by translating the solid curve downward to fit the mica-mica h data, corresponds to $\gamma_h = W_B^0 - W_B^1 = 215 \text{ mJ} \cdot \text{m}^{-2}$. Hence the occluded layer only partially screens out the solid-solid ionic interaction, indicating a relatively weak adsorption energy for water on mica surfaces.

For *healed-misregistered* (h') interfaces, where opposing cleavage halves are mutually rotated through an angle ϕ , the ionic bonding term in the adhesion is strongly influenced by charge-cell overlap. The force and energy in Eqs. (11) and (12) are then modified by a dimensionless angular factor $H(\phi) \leq 1$ (Appendix). A rotation through an angle $\phi \gg \ell/L$, L a characteristic specimen dimension, effectively renders the prospect of encountering like and unlike charge cells at any point across the interface equally probable, in which case we should expect the W_B term in the adhesion to be negated (Appendix). For our h' interfaces (Section II), the experimental rotation angle $\approx 10^\circ$ is indeed well in excess of $\phi = \ell/L \approx 1 \text{ nm}/10 \text{ mm} \approx 6 \times 10^{-6}$ degree evaluated from the above estimate of the cell size. But the h' fracture data points in Figs. 1 to 3, particularly those below RH $\approx 10\%$, do not reduce exactly to the dashed $W = W_{Lap}$ line. The residual increment $W - W_{Lap}$, however small, is more than can be accounted for by van der Waals forces.

This last discrepancy could be explained if the charge distributions in Fig. 8 were to be subject to long-range fluctuations, such that there exist macroscopic "super-domains" of characteristic dimensions $\ell \approx L$. Such domains would manifest themselves as the electrostatic component W_{El} in Eq. (3). For rotations of $\approx 10^\circ$ and specimens of dimension $\approx 10 \text{ mm}$ (Section II), we would need a domain size of $\ell \approx 1 \text{ mm}$ (Appendix), and corresponding charge density $\sigma \approx 0.3 \text{ mC} \cdot \text{m}^{-2}$ (i.e., orders of magnitude smaller than for the short-range cluster in Fig. 8), in Eq. (12) to account for our h' data. Charge domains of this scale have in fact been measured with electrostatic probes on fresh mica cleavage surfaces.⁵ There is also direct evidence, from reversible surface "decoration" experiments¹² before and after exposure of cleavage surfaces to water, that such fluctuations are intrinsic to the mica structure. They have been attributed to some form of "locked-in, long-range correlations" in the aluminum/silicon ion positions in the mica sublattice.³⁹⁻⁴¹ Distinctive manifestations of a macroscopic domain configuration are the highly erratic crack extension in mica in dry conditions (Section II(2)) (reflected in the wide scatter in data at RH $\rightarrow 0$ in Figs. 1 and 5) and triboluminescent emissions in fast fracture.^{3,5,43} It is interesting to note that analogous charge domain structures have been observed in the cleavage of other silicate minerals under ultrahigh vacuum.⁴⁴

For *silica-silica* interfaces, the strongly covalent nature of the siloxane bond precludes much of the long-range effect just described. As indicated in Section III, chemisorptive surface interaction with intrusive water molecules is highly effective in negating the W_B term in Eq. (3). The fact that the adhesion energies for h as well as h' interfaces reduce to a level virtu-

ally coincident with $W = W_{Lap}$ in Fig. 4 further implies that the W_{El} term must also be zero for pure silica-silica interfaces. For soda-lime glass, on the other hand, the h data lie somewhat above $W = W_{Lap}$, suggesting that structural coherency is a factor. In this latter instance, the Na⁺ or Ca²⁺ modifier cations may play a role similar to that envisaged above for the disordered cations in the mica sublattice. Those cations which intersect (or migrate to) the fracture surfaces may be solvated by intrusive water and thereby augment the adhesion by "cationic bridging."²⁶

Unlike Surfaces: In the *mica-silica* system at low RH, a very strong electrostatic component to the adhesion is observed after the surfaces have been brought into contact that is completely absent on the first approach to contact. This electrostatic attraction is quite different from that described for the mica-mica system; it is not the result of "locked-in" charge domains within the surface, but rather is transitory, arising from the transfer of charge from one surface to the other. This transfer results in a charge double layer at the interface which must then be separated when the surfaces are pulled apart; the energy required to separate the charged layers becomes the dominant contribution to W for RH $< 5\%$. Although this effect is seen clearly in both the fracture and adhesion data in Fig. 5, it is in the adhesion experiment that direct measurements of the amount of charge transferred and the resulting force between the surfaces have been made. The remainder of this section will therefore focus on results from the adhesion experiment.

Transferred charge densities in the range 5 to 10 mC·m⁻² have been observed in the contact adhesion experiments,³¹ the silica becoming negatively charged relative to the mica. These densities are higher than those normally observed on an insulating surface as a result of contact with a dissimilar material,⁴⁵ primarily because the smoothness of our silica and mica surfaces allows good microscopic contact at the interface. The charge double layer results in an attraction between the surfaces on the order of 10 MPa for very small (<100 nm) separations, comparable to that observed between parallel capacitor plates carrying the experimentally measured charge densities. This attractive force has a range of several micrometers.

The "lifetime" of the surface charge is a strong function of relative humidity. Measurements with the electrometer (Section III(3)) show that at RH = 1% the charge decays roughly exponentially with a time constant of $5 \times 10^4 \text{ s}$,³¹ an increase in RH to 11% lowers the time constant by almost 2 orders of magnitude, to 650 s. This rapid dissipation at all but the lowest humidities explains the precipitous drop in the observed adhesion energy in Fig. 5 for RH $> 1\%$ to 2%; the charge decays away in the time it takes for the crack to reach its equilibrium length (or, conversely, the decay rate determines the time for the crack to reach a new equilibrium). Like the silica-silica system, the adhesion in humid environments is then dominated by capillary condensation, as is clearly demonstrated by the data in Fig. 5.

(2) Applications to Materials Systems

Let us finally consider the potential relevance of the above results to material systems. We have noted a significant reduction in adhesion between virgin (chemically bonded) and recontacted (physically bonded) interfaces, typically with an order-of-magnitude drop in W . We cite the following examples:

(i) *Coating/Substrate Junctions.* The issue of decohesion is crucial to the mechanical (and other) performance of coatings and thin films. The integrity of a coating that begins to delaminate from an unlike substrate may not be severely compromised if charge transfer occurs across the interface. A relatively strong adhesion would then prevail as long as the delamination process were not so severe that the interface becomes accessible to water vapor.

(ii) *Ceramic-Matrix Composites.* The toughness properties of ceramic-matrix composites are governed in large measure by the energetics of interfaces, e.g., at fiber-matrix pullout⁴⁶ or grain-grain facet sliding boundaries.⁴⁷ In those instances it is not the intrinsic primary chemical forces that determine the ultimate toughness (provided those forces are not too strong that debonding is precluded), but rather the extrinsic frictional forces that control frictional sliding stresses on ensuing fiber or grain pullout. Adhesion forces of the kind described for recontacted interfaces above could play an important role in determining these frictional forces, especially in cases where the contacting surfaces are smooth. These same forces could be augmented by the buildup of transferred charge in dry environments, and by the presence of any strong residual compressive stresses that act to maintain the sliding surfaces in close contact. On the other hand, access to moisture or other interactive species could wash out much of the interaction, in which event the adhesion is controlled by capillary rather than by solid properties.

(iii) *At solid-solid contacts* in tribological processes, adhesion forces may enhance frictional tractions and therefore play a role in the processes of deformation that control friction and wear properties. Events at the sliding interface may be especially disruptive if the accumulation of charge transfer, accompanied by fractoemission ("triboluminescence"), occurs.⁴³

V. Conclusions

We have investigated the factors that contribute to the interface energy of specific like (mica-mica, silica-silica) and unlike (mica-silica) solid-solid interfaces in the presence of water vapor, using brittle fracture and contact adhesion techniques. Particular attention has been paid to interfaces formed by recontacting fully separated surfaces. In those cases the data from the two techniques overlap, within experimental scatter, indicating a complementary process of separation by "sharp-crack propagation."

Comparison of the results for recontacted interfaces with those for virgin and healed-coherent interfaces enables us to distinguish contributions to the adhesion from primary (ionic-covalent) bonding in the virgin structure, electrostatic interactions from macroscopic charge domains, van der Waals forces, and capillary forces from condensed moisture at the near crack tip. For recontacted interfaces in dry atmospheres the electrostatic component, associated with short- and long-range macroscopic charge domains on the opposing surfaces, dominates the adhesion. At mica-mica interfaces, the domains are attributable to disordered cations (aluminum) in the substructure, so that the charge state is "locked in" and reversible. At mica-silica interfaces, an even greater electrostatic interaction (relative to h' mica-mica) arises from wholesale transfer of free charge across the interface. In moist atmospheres capillary condensation acts to screen out or neutralize the electrostatic and primary bonding components, so that, at recontacted interfaces in saturated atmospheres, the capillary term is the only significant contribution.

The relevance of the adhesion states at virgin and recontacted interfaces to certain ceramic properties has been discussed.

APPENDIX

Electrostatic Attraction between Two Misoriented Checkerboards

The electrostatic attraction between two opposing mica surfaces with charge domains was first proposed and calculated by Bryant, Taylor, and Gutshall.⁸ Here we extend the calculation to include the vector nature of the electric field and domain misorientation.

Consider the simple square charge domain structure at the lower, infinite "checkerboard" in Fig. A1. Each domain has sides of length ℓ , and charge density $\pm\sigma$. The electric field at a field point (X, Z, Y) resulting from charges at source points (X', Y', Z') is

$$\vec{E}(X, Z, Y) = \frac{4\sigma}{\pi^3 \epsilon \epsilon_0} \sum_{m,p=0}^{\infty} \frac{(-1)^{m+p}}{a_m b_p} \iint_{-\infty}^{\infty} \frac{\vec{R}}{|\vec{R}|^3} \times \cos\left(\frac{\pi a_m X'}{\ell}\right) \cos\left(\frac{\pi b_p Z'}{\ell}\right) dX' dZ' \quad (\text{A-1})$$

where $a_m = 2m + 1$, $b_p = 2p + 1$, $|\vec{R}|^2 = (X' - X)^2 + (Y' - Y)^2 + (Z' - Z)^2$ with m and p integers. Integration yields the following:

$$\begin{bmatrix} E_X \\ E_Z \\ E_Y \end{bmatrix} = \frac{8\sigma}{\pi^2 \epsilon \epsilon_0} \sum_{m,p=0}^{\infty} \frac{(-1)^{m+p}}{a_m b_p} \times \begin{bmatrix} \frac{a_m}{\lambda_{mp}} \sin\left(\frac{\pi a_m X}{\ell}\right) \cos\left(\frac{\pi b_p Z}{\ell}\right) \\ \frac{a_m}{\lambda_{mp}} \cos\left(\frac{\pi a_m X}{\ell}\right) \sin\left(\frac{\pi b_p Z}{\ell}\right) \\ \cos\left(\frac{\pi a_m X}{\ell}\right) \cos\left(\frac{\pi b_p Z}{\ell}\right) \end{bmatrix} \times \exp\left(-\frac{\pi \lambda_{mp} Y}{\ell}\right) \quad (\text{A-2})$$

where $\lambda_{mp}^2 = a_m^2 + b_p^2$.

Now, a similar, but finite, checkerboard of size $L \times L$ is located parallel to the infinite board at distance Y with domains of opposite signs facing each other. If the domains are rotated through an angle ϕ about the central axis (keeping the board edges fixed), the new in-plane source coordinate system for the charge density function σ becomes (X_ϕ, Z_ϕ) where

$$\begin{bmatrix} X_\phi \\ Z_\phi \end{bmatrix} = \begin{bmatrix} \cos \phi & \sin \phi \\ -\sin \phi & \cos \phi \end{bmatrix} \begin{bmatrix} X \\ Z \end{bmatrix} \quad (\text{A-3})$$

The force per unit area between the two misoriented boards is therefore

$$\begin{aligned} \vec{f}(X, Z, Y, \phi) &= \sigma(X_\phi, Z_\phi, \phi) \vec{E}(X, Z, Y) \\ &= \frac{16\sigma}{\pi^2} \sum_{k,n=0}^{\infty} \frac{(-1)^{k+n}}{a_k b_n} \cos\left[\frac{\pi a_k}{\ell}(X \cos \phi + Z \sin \phi)\right] \\ &\quad \times \cos\left[\frac{\pi a_k}{\ell}(-X \sin \phi + Z \cos \phi)\right] \vec{E}(X, Z, Y) \quad (\text{A-4}) \end{aligned}$$

where $a_k = 2k + 1$, $b_n = 2n + 1$, with k and n integers. (N.B.) Equation (A-4) includes the vector character of the force, which was ignored by Bryant *et al.* The net force per unit area between the two boards is

$$\vec{p}(X, Z, Y, \phi) = \frac{1}{L^2} \iint_{-L/2}^{L/2} \vec{f}(X, Z, Y, \phi) dA \quad (\text{A-5})$$

where $dA = dX dZ$ is an element of the surface area of the finite board. Since $\langle \cos(aX) \sin(bX) \rangle = 0$ for any X , the X and Z components of \vec{p} vanish ($p_X = p_Z = 0$). The resultant force-separation function for the boards is

$$\begin{aligned} p_Y(Y, \phi) &= p_B(Y, \phi) \\ &= \frac{32\sigma^2}{\pi^2 \epsilon \epsilon_0} \sum_{k,n,m,p=0}^{\infty} H_{knmp}(\phi) \exp\left(-\frac{\pi \lambda_{mp} Y}{\ell}\right) \quad (\text{A-6}) \end{aligned}$$

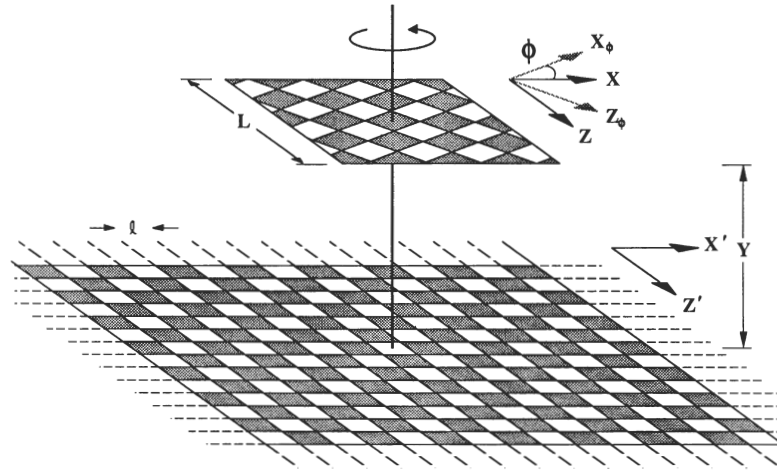


Fig. A1. Charge domains of opposite signs (shaded for negative, open for positive) arranged in a checkerboard pattern on an infinite board (lower) and a finite board (upper) of size $L \times L$. The size of each domain is $\ell \times \ell$. The axes of the domains on the upper board, originally aligned with the board axes (X, Y), are rotated by an angle ϕ to (X_ϕ, Y_ϕ) about a central axis.

where

$$\begin{aligned}
 H_{knmp}(\phi) &= \frac{4}{L^2} \iint_{-L/2}^{L/2} \frac{(-1)^{k+n+m+p}}{a_k b_n a_m b_p} \\
 &\times \cos\left(\frac{\pi a_m X}{\ell}\right) \cos\left(\frac{\pi b_p Z}{\ell}\right) \\
 &\times \cos\left[\frac{\pi a_m}{\ell}(X \cos \phi + Z \sin \phi)\right] \\
 &\times \cos\left[\frac{\pi b_n}{\ell}(-X \sin \phi + Z \cos \phi)\right] dX dZ \\
 &= \frac{(-1)^{k+n}}{a_m^2 a_k b_n} \{j_0[(\alpha + \beta - \gamma)\xi] \\
 &\quad + j_0[(\alpha + \beta + \gamma)\xi]\} \\
 &\quad \times \{j_0[(\alpha - \beta - \gamma)\xi] + j_0[(\alpha - \beta + \gamma)\xi]\}
 \end{aligned} \tag{A-7}$$

and $\alpha = \pi a_k \cos \phi$, $\beta = \pi b_n \sin \phi$, $\gamma = \pi a_m$, $\xi = L/\ell$, with $j_0(x)$ the 0th-order spherical Bessel function (i.e., $j_0(x) = (\sin x)/x$).

The interfacial energy is found by integrating p_Y from b_0 to infinity,

$$W_B(\phi) = \frac{32\sigma^2\ell}{\pi^3\epsilon\epsilon_0} \sum_{k,n,m,p=0}^{\infty} \frac{H_{knmp}(\phi)}{\lambda_{mp}} \exp\left(-\frac{\pi\lambda_{mp}b_0}{\ell}\right) \tag{A-8}$$

This series converges rapidly due to the presence of the exponential term, so only the first term with $k = n = m = p = 0$ is important, i.e.,

$$\begin{aligned}
 p_B(Y, \phi) &\approx H(\phi) \left[\frac{32\sigma^2}{\pi^2\epsilon\epsilon_0} \exp\left(-\frac{\sqrt{2}\pi Y}{\ell}\right) \right] \\
 &= H(\phi) p_B(Y, 0)
 \end{aligned} \tag{A-9}$$

$$\begin{aligned}
 W_B(\phi) &\approx H(\phi) \left[\frac{16\sqrt{2}\sigma^2\ell}{\pi^3\epsilon\epsilon_0} \exp\left(-\frac{\sqrt{2}\pi b_0}{\ell}\right) \right] \\
 &= H(\phi) W_B(0)
 \end{aligned} \tag{A-10}$$

where

$$\begin{aligned}
 H(\phi) &= H_{0000}(\phi) \\
 &= \{j_0[(\cos \phi + \sin \phi - 1)\pi\xi] \\
 &\quad + j_0[(\cos \phi + \sin \phi + 1)\pi\xi]\} \\
 &\quad \times \{j_0[(\cos \phi - \sin \phi - 1)\pi\xi] \\
 &\quad + j_0[(\cos \phi - \sin \phi + 1)\pi\xi]\}
 \end{aligned} \tag{A-11}$$

Thus the dependence of both the force separation function and the interfacial energy on the misorientation angle ϕ is governed predominately by the function $H(\phi)$. Plots of H vs ϕ are shown in Fig. A2 for $\xi = 5$ and $\xi = 20$. Note that H drops rapidly once ϕ deviates from $\phi = 0$. The angle when H first drops to zero for a specific ξ is denoted by ϕ^* . Figure A3 plots ϕ^* vs ξ . For $\phi = 0$, $H(\phi) = 1$, Eqs. (A-9) and (A-10) give us Eqs. (11) and (12) in the text.

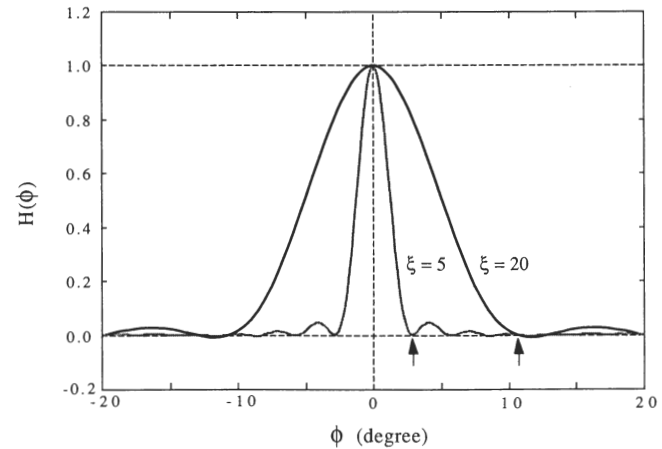


Fig. A2. Plot of $H(\phi)$ vs ϕ for $\xi = 5$ and $\xi = 20$.

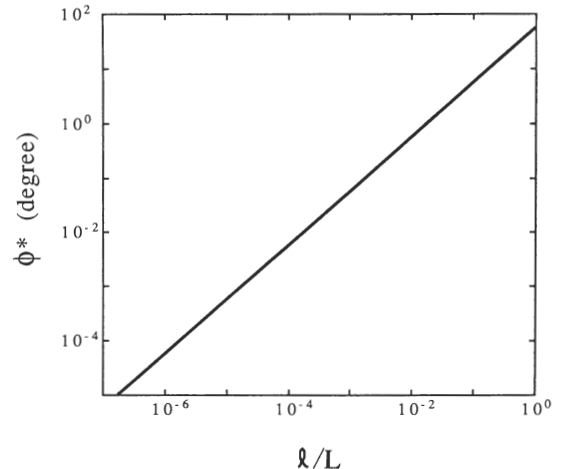


Fig. A3. Plot for ϕ^* vs ℓ/L .

Acknowledgments: We acknowledge many stimulating discussions with R. G. Horn and with E. R. Fuller, Jr., and W. C. Carter, especially with regard to the calculations in the Appendix.

References

- ¹R. G. Horn, "Surface Forces and Their Action in Ceramic Materials," *J. Am. Ceram. Soc.*, **73** [5] 1117–35 (1990).
- ²A. W. Adamson, *Physical Chemistry of Surfaces*. Wiley, New York, 1982.
- ³J. W. Obreimoff, "The Splitting Strength of Mica," *Proc. R. Soc. London*, **A127** [805] 290–97 (1930).
- ⁴B. V. Derjaguin, N. A. Krotova, and V. V. Karasev, "Electrical Phenomena in the Disruption Mechanism of Some Solids," *Sov. Phys.—Dokl. (Engl. Transl.)*, **1** [4] 466–69 (1956).
- ⁵B. V. Derjaguin and M. S. Metsik, "Role of Electrical Forces in the Process of Splitting Mica Along Cleavage Planes," *Sov. Phys.—Solid State (Engl. Transl.)*, **1** [10] 1393–99 (1960).
- ⁶A. I. Bailey, "Friction and Adhesion of Clean and Contaminated Mica Surfaces," *J. Appl. Phys.*, **32** [8] 1407–12 (1961).
- ⁷P. J. Bryant; pp. 311–13 in *Transactions of the Ninth National Vacuum Symposium*. Macmillan, New York, 1962.
- ⁸P. J. Bryant, L. H. Taylor, and P. L. Gutshall; pp. 21–26 in *Transactions of the Tenth National Vacuum Symposium*. Macmillan, New York, 1963.
- ⁹A. I. Bailey and S. M. Kay, "A Direct Measurement of the Influence of Vapor, of Liquid and of Oriented Monolayers on the Interfacial Energy of Mica," *Proc. R. Soc. London*, **A301** [1464] 47–56 (1967).
- ¹⁰A. I. Bailey and A. G. Price, "Interfacial Energies of Monomolecular Films of Fatty Acids Deposited on Mica in Aqueous and Nonaqueous Media—The Strength of Hydrophobic Interactions," *J. Chem. Phys.* **53** [9] 3421–27 (1970).
- ¹¹R. B. Leonasio, "Fracture and Healing Effects in Mica Crystals," *J. Am. Ceram. Soc.*, **55** [9] 437–39 (1972).
- ¹²M. S. Metsik, "Splitting of Mica Crystals and Surface Energy," *J. Adhes.*, **3** [4] 307–14 (1972).
- ¹³A. I. Bailey and H. Daniels, "The Determination of the Intermolecular Forces of Attraction between Macroscopic Bodies for Separations down to the Contact Point," *J. Phys. Chem.*, **77** [4] 501–15 (1973).
- ¹⁴B. R. Lawn, D. H. Roach, and R. M. Thomson, "Thresholds and Reversibility in Brittle Cracks: An Atomistic Surface Force Model," *J. Mater. Sci.*, **22** [11] 4036–50 (1987).
- ¹⁵B. R. Lawn and S. Lathabai, "Surface Forces and Fracture in Brittle Materials," *Mater. Forum*, **11**, 313–22 (1988).
- ¹⁶K.-T. Wan, N. Aimard, S. Lathabai, R. G. Horn, and B. R. Lawn, "Interfacial Energy States of Moisture-Exposed Cracks in Mica," *J. Mater. Res.*, **5** [1] 172–82 (1990).
- ¹⁷K. L. Johnson, K. Kendall, and A. D. Roberts, "Surface Energy and the Contact of Elastic Solids," *Proc. R. Soc. London*, **A324** [1558] 301–13 (1971).
- ¹⁸B. V. Derjaguin, V. M. Muller, and Yu. P. Toporov, "Effect of Contact Deformations on the Adhesion of Particles," *J. Colloid Interface Sci.*, **53** [2] 314–26 (1975).
- ¹⁹A. Fogden and L. R. White, "Contact Elasticity in the Presence of Capillary Condensation: I. The Nonadhesive Hertz Problem," *J. Colloid Interface Sci.*, **138** [2] 414–30 (1990).
- ²⁰D. Maugis and M. Barquins, "Fracture Mechanics and the Adherence of Viscoelastic Bodies," *J. Phys. D*, **11** [14] 1989–2023 (1978).
- ²¹J. N. Israelachvili, *Intermolecular and Surface Forces*; Ch. 14. Academic Press, London, U.K., 1985.
- ²²R. G. Horn, J. N. Israelachvili, and F. Pribac, "Measurement of the Deformation and Adhesion of Solids in Contact," *J. Colloid Interface Sci.*, **115** [2] 480–92 (1987).
- ²³H. Christenson, "Adhesion between Surfaces in Undersaturated Vapors—A Reexamination of the Influence of Meniscus Curvature and Surface Forces," *J. Colloid Interface Sci.*, **121** [1] 170–78 (1988).
- ²⁴P. M. McGuigan and J. N. Israelachvili, "Adhesion and Short-Range Forces Between Surfaces. Part II: Effects of Surface Lattice Mismatch," *J. Mater. Res.*, **5** [10] 2232–43 (1990).
- ²⁵K.-T. Wan and B. R. Lawn, "Surface Forces at Crack Interfaces in Mica in the Presence of Capillary Condensation," *Acta Metall.*, **38** [11] 2073–83 (1990).
- ²⁶H. M. Michalske and E. R. Fuller, "Closure and Repropagation of Healed Cracks in Silicate Glass," *J. Am. Ceram. Soc.*, **68** [11] 586–90 (1985).
- ²⁷R. G. Horn and D. T. Smith, "Contact Electrification and Adhesion between Dissimilar Materials"; in preparation.
- ²⁸R. G. Horn, D. T. Smith, and W. Haller, "Surface Forces and Viscosity of Water Measured between Silica Sheets," *Chem. Phys. Lett.*, **162** [4, 5] 404–408 (1989).
- ²⁹J. W. Hutchinson, "Mixed-Mode Fracture Mechanics of Interfaces," *Acta-Ser. Metall. Proc. Ser.*, **4**, 295–306 (1990).
- ³⁰D. T. Smith and R. G. Horn, "Surface Forces and Adhesion between Dissimilar Materials Measured in Various Environments," *Mater. Res. Soc. Symp. Proc.*, **170**, 3–9 (1990).
- ³¹D. T. Smith, "Measuring Contact Charge Transfer at Interfaces: A New Experimental Technique," *J. Electrostat.*, **26** [3] 291–308 (1991).
- ³²S. M. Wiederhorn, "Fracture Surface Energy of Glass," *J. Am. Ceram. Soc.*, **52** [2] 99–105 (1969).
- ³³S. M. Wiederhorn and L. H. Bolz, "Stress Corrosion and Static Fatigue of Glass," *J. Am. Ceram. Soc.*, **53** [10] 543–48 (1970).
- ³⁴K.-T. Wan, S. Lathabai, and B. R. Lawn, "Crack Velocity Functions and Thresholds in Brittle Solids," *J. Eur. Ceram. Soc.*, **6** [4] 259–68 (1990).
- ³⁵B. Stavrinidis and D. G. Holloway, "Crack Healing in Glass," *Phys. Chem. Glasses*, **24** [1] 19–25 (1983).
- ³⁶B. V. Derjaguin, N. V. Churaev, and V. M. Muller, *Surface Forces*. Consultants Bureau, New York, 1987.
- ³⁷D. R. Clarke, B. R. Lawn, and D. H. Roach, "The Role of Surface Forces in Fracture"; pp. 341–50 in *Fracture Mechanics of Ceramics*, Vol. 8. Edited by R. C. Bradt, A. G. Evans, D. P. H. Hasselman, and F. F. Lange. Plenum Press, New York, 1986.
- ³⁸J. Mahanty and B. W. Ninham, *Dispersion Forces*. Academic Press, London, U.K., 1976.
- ³⁹R. F. Giese; in *Reviews in Mineralogy*, Vol. 13, *Micas*; Ch. 4. Mineralogical Society of America, Chelsea, MI, 1984.
- ⁴⁰S. W. Bailey; in *Reviews in Mineralogy*, Vol. 13, *Micas*; Chs. 1 and 2. Mineralogical Society of America, Chelsea, MI, 1984.
- ⁴¹S. W. Bailey, "Reviews of Cation Ordering in Micas," *Clays Clay Miner.*, **32** [2] 81–92 (1984).
- ⁴²J. E. Lennard-Jones and B. M. Dent, "Cohesion at a Crystal Surface," *Trans. Faraday Soc.*, **24**, 92–108 (1928).
- ⁴³J. T. Dickinson, E. E. Donaldson, and M. K. Park, "The Emission of Electrons and Positive Ions from Fracture of Materials," *J. Mater. Sci.*, **16** [10] 2897–908 (1981).
- ⁴⁴J. A. Ryan, J. J. Grossman, and W. M. Hansen, "Adhesion of Silicates Cleaved in Ultrahigh Vacuum," *J. Geophys. Res.*, **73** [18] 6061–70 (1968).
- ⁴⁵For a detailed review of contact electrification, see J. Lowell and A. C. Rose-Innes, "Contact Electrification," *Adv. Phys.*, **29** [6] 947–1023 (1980).
- ⁴⁶A. G. Evans, "Perspective on the Development of High-Toughness Ceramics," *J. Am. Ceram. Soc.*, **73** [2] 187–206 (1990).
- ⁴⁷S. J. Bannison and B. R. Lawn, "Role of Interfacial Grain-Bridging Sliding Friction in the Crack-Resistance and Strength Properties of Nontransforming Ceramics," *Acta Metall.*, **37** [10] 2659–71 (1989). □